

Received June 3, 2020, accepted June 8, 2020, date of publication June 10, 2020, date of current version June 25, 2020.

Digital Object Identifier 10.1109/ACCESS.2020.3001337

# Detecting Total Electron Content Precursors Before Earthquakes by Examining Total Electron Content Images Based on Butterworth Filter in Convolutional Neural Networks

JYH-WOEI LIN<sup>1</sup> AND JUING-SHIAN CHIOU<sup>2</sup>

<sup>1</sup>Binjiang College, Nanjing University of Information Science and Technology, Wuxi 214105, China

<sup>2</sup>Department of Electrical Engineering, Southern Taiwan University of Science and Technology, Tainan 71005, Taiwan

Corresponding author: Juing-Shian Chiou (jschiou@stust.edu.tw)


This work was supported by the Ministry of Science and Technology, Taiwan, under Grant MOST 108-2221-E-218-028.

**ABSTRACT** Daily total electron content (TEC) images created by splitting TEC maps for three time periods from September 1 to 24, 1999; from February 1 to 24, 2003; and from May 1 to 24, 2003 (Taiwan Standard Time [TST]) as training images (inputs) were used to create two convolutional neural network (CNN) models. However, splitting the TEC maps of the three time periods into daily TEC images caused wedge effects. The wedge effects were reduced using a low-pass filter called the Butterworth filter. This resulted in clearer TEC precursors for earthquakes, facilitating the identification of earthquakes of magnitude  $M_w \geq 5.0$  that exhibited associated TEC precursors during three periods, particularly for the Chi-Chi earthquake of September 21, 1999. The results of this study were compared with those of Lin *et al.* and Lin associated with the Chi-Chi earthquake. Simultaneously, two CNN models that were developed were verified to be rational due to the high accuracy of their predictions. These two models were used to verify each other's accuracies and to demonstrate the reliability of the method in this study. Therefore, statistical analysis was not the aim. The final outputs of the two CNN model were defined as similarities. Similarities, which are larger than 0.5, were defined as TEC precursors of earthquakes. TEC precursors described as temporal TEC multi-precursors (TTMPs) by Zoran *et al.* were detectable on the 1st, 3rd, and 4th days (that is, on September 17, 18, and 20, 1999, respectively) prior to the Chi-Chi earthquake of September 21, 1999. These results are consistent with those of Liu *et al.* and Lin. A TEC precursor on May 13, 2003, (TST) was detectable 2 days prior to the earthquake on May 15, 2003, (TST) with the magnitude ( $M_w$ ) of 5.52. The low standard deviation (STD) and mean square error (MSE) confirm the reliability of both CNN models. Regarding mechanical principles, the TTMPs related to the Chi-Chi earthquake were caused by an electric field. The cause of the TEC precursor on May 13, 2003, prior to the earthquake on May 15, 2003, was an argument without any corresponding study for comparison.

**INDEX TERMS** Daily total electron content (TEC) images, convolutional neural network (CNN), wedge effects, Butterworth filter, temporal TEC multi-precursors (TTMPs), Chi-Chi earthquake, standard deviation (STD), mean square error (MSE).

## I. INTRODUCTION

Many studies have researched the total electron content (TEC) anomalies associated with large earthquakes [64], [44], [61], [25], [39], [57]. Wang *et al.* [64] predicted seismoionospheric TEC disturbances before an earthquake. The

The associate editor coordinating the review of this manuscript and approving it for publication was Gerardo Di Martino .

TEC data were extracted using data mining to obtain the features of preseismic ionospheric anomalies. Liu *et al.* [44] detected TEC precursors from 1 day before the Sumatra Indonesia  $M_w$  7.2 earthquake that occurred on July 5, 2005. Tao *et al.* [61] identified a TEC anomaly from 2 days before the  $M_w$  7.7 earthquake south of Java on July 17, 2006. Ho *et al.* [25] described seismoionospheric TEC anomalies preceding 49 earthquakes with  $M_w \geq 6.5$  in 2010 in Chile.

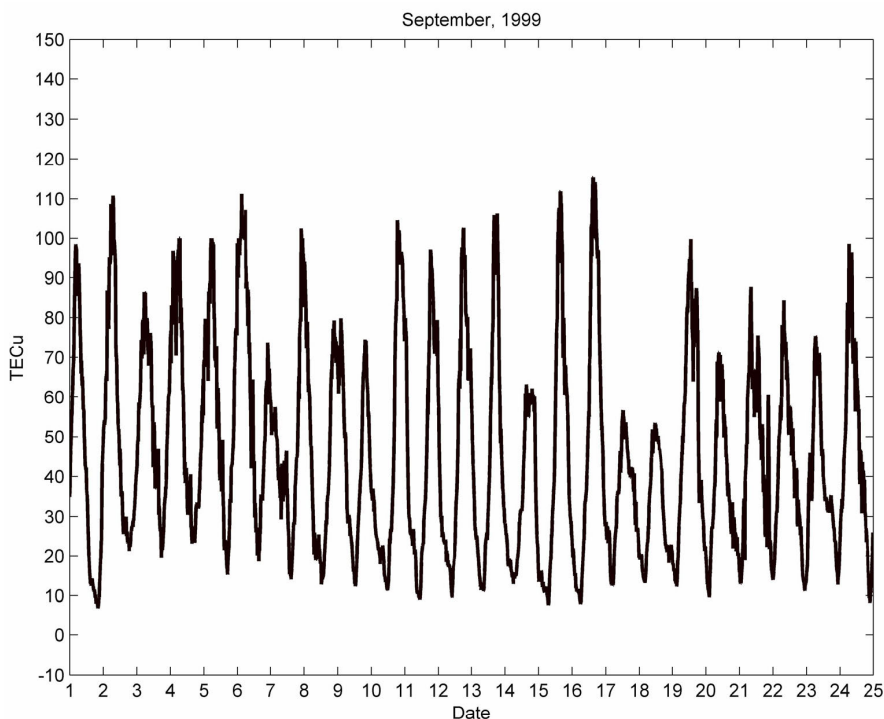


**FIGURE 1.** TEC maps from September 1 to 24, 1999 (TST). The Chi-Chi earthquake occurred at 01:47:15 on September 21, 1999 (TST) with the epicenter at 23.85° N and 120.82° E, at a depth of 8.00 km and with the magnitude ( $M_w$ ) = 7.60 (CWB).

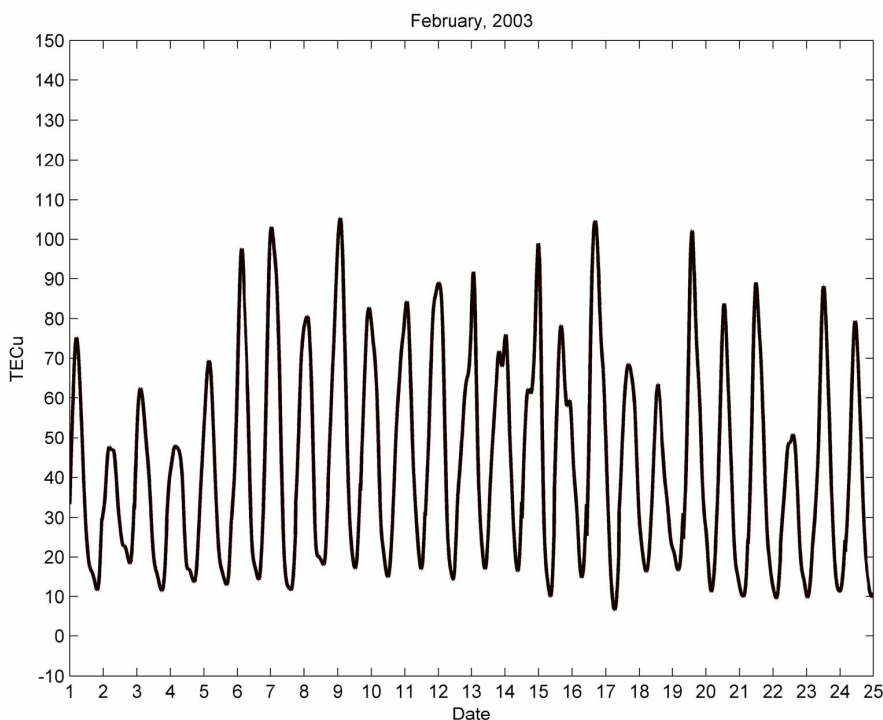


**FIGURE 2.** TEC maps from February 1 to 24, 2003 (TST). No earthquakes occurred with the magnitude ( $M_w$ )  $\geq 5.0$  in this time period.

Lin *et al.* [39] predicted TEC precursors constituting spatial TEC multi-precursors (STMPs) prior to the China Ludian earthquake at 08:30:13 UT on August 3, 2014

( $M_w = 6.1$ ) using Kernel-based two-dimensional principal component analysis through examination of the ionospheric two-dimensional TEC variations obtained from the

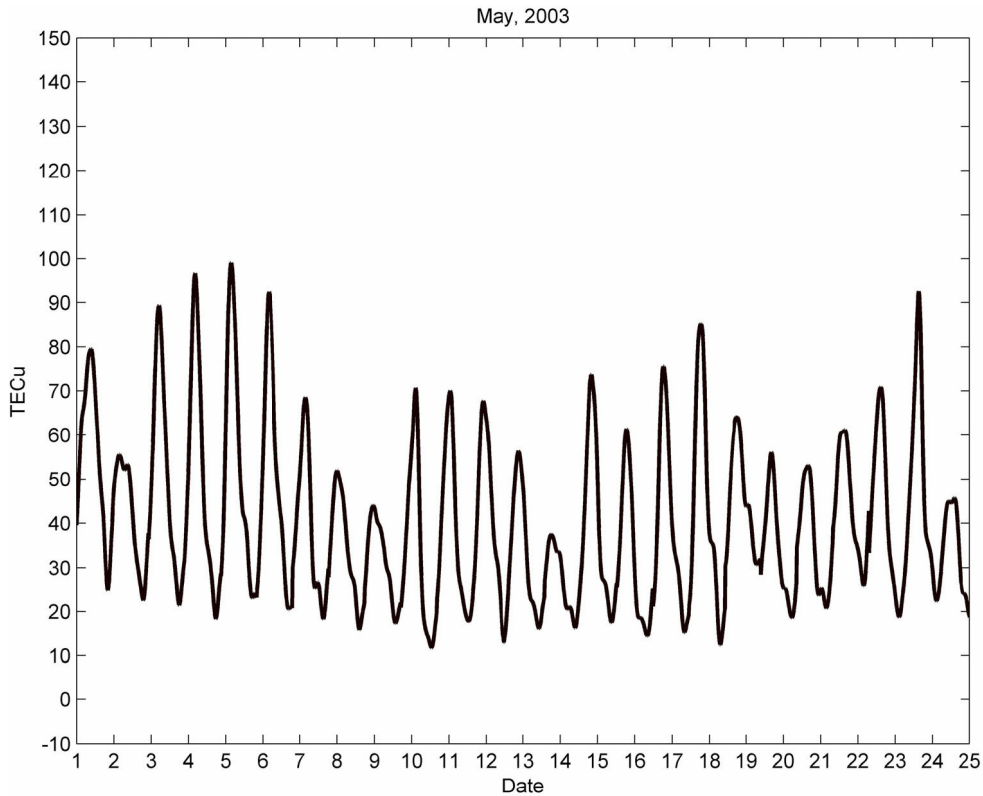


**FIGURE 3.** TEC maps from May 1 to 24, 2003 (TST). An earthquake occurred at 09:17:42 on May 15, 2003 (TST) with an epicenter at  $25.06^{\circ}$  N and  $122.52^{\circ}$  E, at a depth of 17.58 km and the magnitude ( $M_w$ ) = 5.52.

NASA Global Differential Global Positioning System network. Shah *et al.* [57] detected TEC variations in the ionosphere associated with the  $M_w$  7.7 Chile earthquake on November 14, 2007. However, they did not use the neural network (NN) as their tool.

Artificial neural networks (ANNs) such as convolutional neural networks (CNNs) have been successfully used as recognition methods and for earthquake magnitude prediction [38], [69]. The researched results were better than those of other studies. Perol *et al.* [50] researched seismicity in the Central United States to improve seismic hazard assessment and detect earthquake locations using CNN. However, this study did not assess the precursor of larger earthquakes.

Akhoondzadeh [5] detected TEC and thermal anomalies using an adaptive network-based fuzzy inference system for the earthquake with an  $M_w$  of 6.4 on August 11, 2012, in NW Iran. Akhoondzadeh [6] detected TEC signal variations as the precursors for the earthquake with an  $M_w$  of 7.7 in Iran on April 16, 2013, by combining ANNs and particle swarm optimization. This study also compared the results with those from the mean, median, wavelet, Kalman filter, autoregressive integrated moving average, support vector machine, and genetic algorithm (GA) methods. The combined method provided a new tool for the detection of thermal and TEC seismic anomalies. Sompota *et al.* [56] used ANNs to determine ionospheric TEC anomalies as ionospheric precursors of

large earthquakes and, by combining ANNs with the Kriging method, to estimate the epicenter area. Sabzehee *et al.* (2018) performed an ANN and multilayer perceptron for pattern recognition and prediction of TEC variations in the seismicity area in Iran. TEC changed their special recognition as earthquake ionospheric precursor. Classic methods such as the mean method failed to detect nonlinear TEC patterns because TEC exhibited complex and nonlinear behavior.

Aji *et al.* [4] detected earthquake TEC precursors in Sumatra using the N-Model Neural Network Model. That study also used the disturbance storm time index to account for the effects of geomagnetic storms on TEC. Therefore, the method could identify earthquake precursors, providing a potential warning system for early detection of earthquakes. Hanzaei [22] used three standard, classical, and intelligent methods including the median, Kalman filter, and ANN methods to detect potential unusual TEC variations as precursors to the Mexico earthquake with an  $M_w$  of 8.2 at 04:49:19 UTC on September 8, 2017. However, seismicity was difficult to establish because of the complex behavior of the ionosphere. Song *et al.* [58] applied NNs to develop a regional TEC prediction model for China. The traditional NN-based model and GA were utilized to optimize the initial weights of NN. The NN had 19 input parameters that clearly caused variations in ionospheric parameters. These parameters included ionospheric diurnal

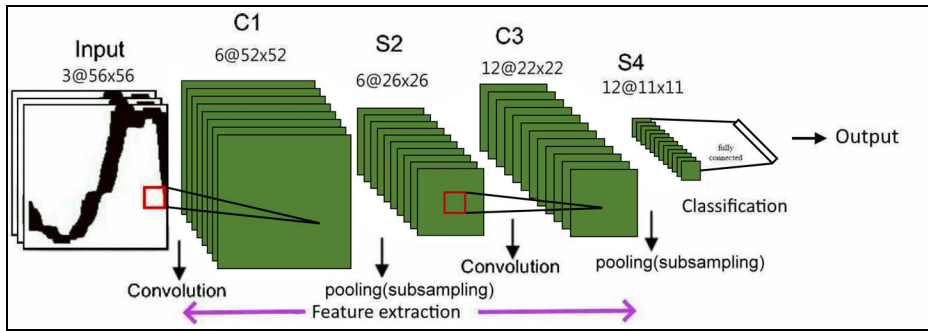


**FIGURE 4.** Framework of a two-dimensional CNN with two hidden layers. For example, the symbol “6@” means six feature maps with the concept of neurons to be generated after convolution called the actions using a filter [26]. Pooling is the subsampling of feature maps to reduce the computing time. Using the algorithmic called fully-connected in fully connected layers, the daily TEC images as inputs are classified called classification to identify TEC precursors of earthquakes in this study.

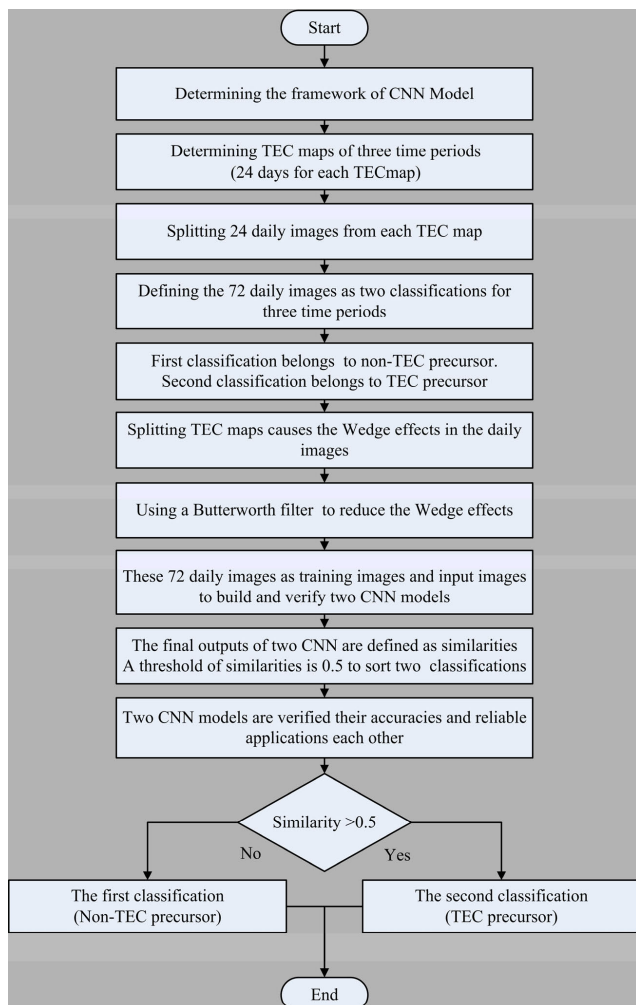


**FIGURE 5.** Procedure for creating a CNN model.

variations, seasonal information, solar cycle, geomagnetic activities, geographic coordinates, and declination. The output parameter was the daily TEC measured from 43 permanent Global Positioning System stations in China. The TEC data during 2012–2014 served as training data. For NN

model verification, the TEC data in 2015 were selected as the test data. Predicted results of the GA-based NN (GA-NN) model, backpropagation-based NN model, and International Reference Ionosphere 2012 model were used for comparison. Finally, the GA-NN model demonstrated promise for applications in ionospheric studies. By using median, Kalman filter, and NN methods, Akhoondzadeh *et al.* [7] recorded a TEC precursor 9 days before the earthquake with an  $M_w$  value of 7.3 near the Iran–Iraq border in west Iran (34.911°N, 45.959°E) that occurred at 18:18:17 UTC on November 12, 2017. The Kalman filter and NNs were used to detect another clear anomaly 11 days before this earthquake at 16:00 UTC. Research methods used in other studies are overly complicated, sometimes requiring the application of multiple methods and more TEC data to enhance the computing time. TEC variance was easily affected by the space weather (e.g., the planetary k index [kp index]), which should be considered in the evaluation [39]. TEC seasonal variations also should be considered [27]. Their research results had the major problem regarding the determination of accurate TEC precursors for large earthquakes. When kp indices are too large (>4) [9], geomagnetic storms are induced, which interfere with and affect TEC variances. Therefore, an error is caused to determine correct and true TEC precursors related to large earthquakes. This represents a major shortcoming of other studies.

CNN has been demonstrated to constitute a powerful and suitable tool for image classification [35], [71], [33], [40]. Therefore, the objective of this study is to detect TEC precursors of larger earthquakes by using a CNN (for convenience, the abbreviation “CNN” means two-dimensional CNN in this study) through the examination of TEC maps instead of TEC data to confirm TEC precursors of the Chi-Chi earthquake of September 21, 1999 and compare the results with those in the studies of Lin [36] and Liu *et al.* [41]. Simultaneously, the accuracy and rationality of the researched results and analysis using CNN are verified. The research in this study uses image classifications but not statistical analysis.

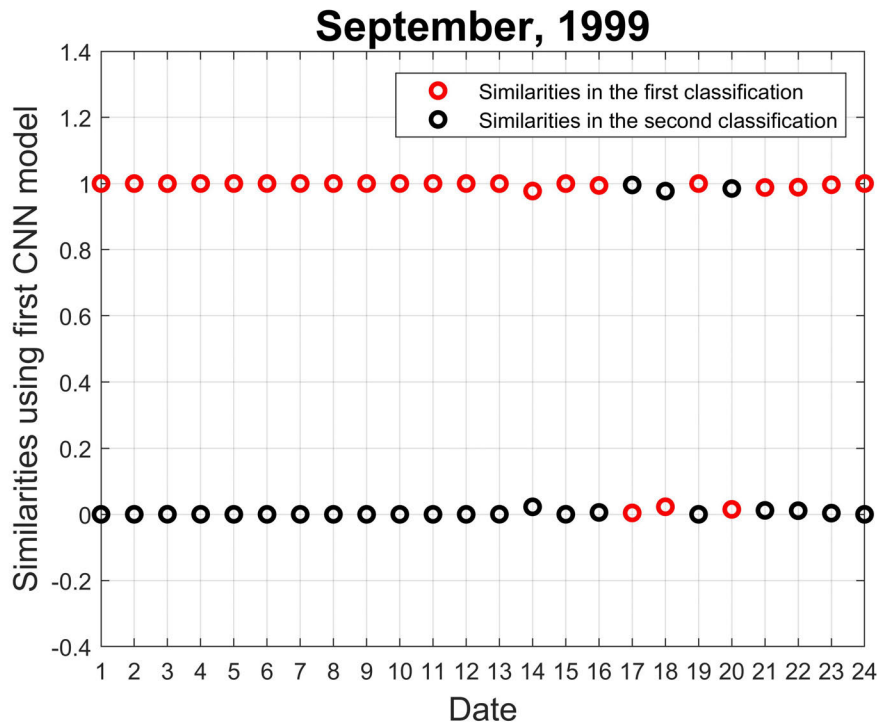


FIGURE 6. Visual presentation of Table 1.

**Some factors** require no consideration in this study. These factors include geological environments around earthquake epicenter, geological averment variance for large time scales (e.g., the slip rate of the Philippine Sea Plate related to the Eurasian Plate), kp index (indicating geomagnetic variances such as the aforementioned geomagnetic storms), and TEC seasonal variations [1], [2], [38], [27]. The information on these factors is assimilated into the TEC maps examined, which serve as training images for a CNN model. Therefore, some solar-geomagnetic data are omitted in this study. The text files of TEC data may not be obtained from the data source, meaning that only TEC maps can be acquired from the data source. The text files of TEC data can be obtained through data mining. Data mining is more complicated [64]. Therefore, data mining is not necessary to perform in this study. Simultaneously, high-resolution TEC maps are not required. The waveform patterns in TEC maps can be directly identified and classified using CNN with a suitable resolution by reducing the resolution to shorten the image processing time without considering the characteristics of spotty, irregular, and nonstationary of TEC data sets [22], which is assigned to a special classification. Subsequently, if this special classification is associated with the classification for earthquake-associated TEC anomalies, then the waveform pattern can be identified as a TEC precursor. However, using this CNN method of classification to identify TEC precursors presents a problem regarding the cross-matching of different image types. TEC map processing is straightforward. Therefore, the method used in this study overcomes the

shortcomings of those used in other studies. The TEC maps used in this study can be acquired from other literatures with copyright permission. Moreover, no similar studies have been published yet. Therefore, a new proposal is presented in this study. Finally, two prominent considerations merit mention. This research involves the use of daily TEC images through the splitting of TEC maps. Such splitting of inputs causes wedge effects [54], a type of artificial image processing errors. Thus, for these split images, a low pass filter is applied to reduce wedge effects before the convolutional layers in the first hidden layer. Addressing the aforementioned factors to compare and identify the TEC waveforms for TEC images obtained daily using CNN is another crucial consideration. Therefore, this study demonstrates that the creation of a CNN model for the identification of TEC precursors is uncomplicated without numerous TEC maps as training images.

## II. DATA SOURCE

The TEC data of global positioning system (GPS) ionospheric maps are from the Chung-Li station (25.00° N and 121.20° E) of ground network stations of the ionospheric observatory for the Central Weather Bureau (CWB) in Taiwan. The ionospheric TEC maps examined at this station reflect the seismic activity of Taiwan called Chung-Li Ionosonde. Liu *et al.* [41] examined TEC data to detect the TEC precursors on the 1st, 3rd, and 4th days prior to the Chi-Chi earthquake of September 21, 1999 using the Chung-Li Ionosonde. For simultaneous observation of



**TABLE 1.** Similarities in the first and second classifications for the time period in Fig. 1 using the first CNN model. STD = 0.012, MSE = 0.014.

Day, September, 1999 (TST)	Similarities in the first classification	Similarities in the second classification
1	1.0000	0.0000
2	0.9999	0.0001
3	0.9997	0.0003
4	0.9999	0.0001
5	1.0000	0.0000
6	1.0000	0.0000
7	1.0000	0.0000
8	1.0000	0.0000
9	1.0000	0.0000
10	1.0000	0.0000
11	1.0000	0.0000
12	1.0000	0.0000
13	0.9997	0.0003
14	0.9773	0.0227
15	0.9998	0.0002
16	0.9942	0.0058
<b>17</b>	<b>0.0043</b>	<b>0.9957</b>
<b>18</b>	<b>0.0229</b>	<b>0.9771</b>
19	0.9999	0.0001
<b>20</b>	<b>0.0150</b>	<b>0.9850</b>
21	0.9880	0.0120
22	0.9889	0.0111
23	0.9963	0.0037
24	1.0000	0.0000

large areas of the ionosphere, recordings from a network of ground-based stations are ideally used. TEC data from a point (25.00° N, 121.20° E) located at Chung-Li are derived and estimated from ground-based GPS stations to monitor variations in the ionosphere in Taiwan through VHF radar echoes emitted by the Chung-Li VHF radar station (24.91° N, 121.24° E), that is, the so-called Chung-Li Ionosonde. Ionospheric disturbances can be monitored with a radius 500 km from the Chung-Li Ionosonde. Therefore, the TEC data attributes belong to the Chung-Li Ionosonde, and the TEC data are estimated using this Ionosonde combined with the receiver system of the VHF radar station. The estimated TEC data therefore have a high level of accuracy. The procedure of this combined system is complex to explain for estimating TEC data that is not an issue in this study. A number of relevant studies exist [16], [41], [42], [63], [46], [52], [43], [32], [37], [14], [21], [13], [45], [62], [65].

TEC maps for three time periods are used in this study. They are from September 1 to 24, 1999 (Fig. 1); February 1 to 24, 2003 (Fig. 2); and May 1 to 24, 2003 (Fig. 3) (Taiwan Standard Time [TST]). Earthquake catalogs with

the magnitudes ( $M_w$ )  $\geq 5.0$  during three time periods are examined. The Chi-Chi earthquake occurred at 01:47:15 on September 21, 1999 (TST) with the epicentre at 23.85° N and 120.82° E, at a depth of 8.00 km, and with the magnitude ( $M_w$ ) = 7.60 [34] (CWB). Another earthquake occurred at 09:17:42 on May 15, 2003 (TST) with its epicentre at 25.06° N and 122.52° E, at a depth of 17.58 km, and with the magnitude ( $M_w$ ) = 5.52 (CWB). The TEC precursors of the two earthquakes are detected with CNN. The distances from Chung-Li Ionosonde station to the epicenters of two earthquakes are about 111km and 110km, respectively (CWB). The epicenters locate within the range the Chung-Li Ionosonde. There are only two earthquakes with the magnitudes ( $M_w$ )  $\geq 5.0$  in the three time periods as stated previously. This is the reason that the three time periods are selected.

### III. CONVOLUTIONAL NEURAL NETWORK

The hidden layers of a convolutional neural network (CNN) typically consist of convolutional layers, subsampling layers, fully connected layers, and normalization layers, as shown in

TABLE 2. Similarities in the first and second classifications for the time period in Fig. 2 using the first CNN model. STD = 0.162, MSE = 0.026.

Day, February, 2003	First classification	Second classification
1	0.9936	0.0064
2	0.9710	0.0290
3	0.9879	0.0121
4	0.8997	0.1003
5	0.9454	0.0546
6	0.9979	0.0021
7	0.9981	0.0019
8	0.7999	0.2001
9	0.8300	0.1700
10	0.9689	0.0311
11	0.6879	0.3121
12	0.9999	0.0001
13	0.9899	0.0101
14	0.9423	0.0577
15	0.7368	0.2632
16	0.7286	0.2714
17	0.7881	0.2119
18	0.7464	0.2536
19	0.9990	0.0010
20	0.9457	0.0543
21	0.7856	0.2144
22	0.8856	0.1144
23	0.9976	0.0024
24	0.8591	0.1409

Fig. 4 [3]. Several studies and engineering applications have indicated that a NN of two hidden layers with few neurons can replace a network with numerous neurons in a hidden layer [68], [26], [28], [24], [60], [66], [15], [18]. In the study, the framework of CNN with two hidden layers is performed as in Fig. 4.

The mathematical of CNN is briefly introduced in this section. A normalization layer normalizes each input image across a minibatch for each hidden layer, and this is termed Batch normalization [3]. Batch normalization can accelerate training of CNN and reduces sensitivity to network initialization. In the convolution layers in the first hidden layer, for the  $j$ th output image  $Y_j^L$

$$Y_j^L = f\left(\sum_{i=1}^N X_i^{L-1} * K_{i,j}^L + b_j^L\right) \quad (1)$$

where the symbol X represents input images, and the superscript L represents the positions of hidden layers. For example,  $L = 1$  represents the first hidden layer.

The symbol N represents the number of input images, the subscript i represents the  $i$ th input image. K is kernel

called filter, which is convolved with input images with the symbol “\*” [26]. The symbols b and f represent bias and the activation function, respectively. The normal activation function is used. It is a sigmoid function, and its range is between 0 and 1 as follows [31]:

$$f(t) = \frac{1}{1 + e^{-t}} \quad (2)$$

The algorithm of the subsampling layer, termed polling for the same hidden layer, is as follows:

$$Z_j^{L+1} = FC[f(B_j^{L+1} \text{down}_n(Y_j^L) + b_j^{L+1})] \quad (3)$$

where  $B_j^{L+1}$  is the multiplicative bias for  $Y_j^L$ . The word “ $\text{down}_n$ ” is called the subsampling function, which is used to subsample  $Y_j^L$  with summing over an n-by-n block, so that the output image  $Z_j^{L+1}$  exhibits an n-times smaller spatial resolution. Subsequently,  $Z_j^{L+1}$  is the input image for the next hidden layer. The symbol “FC” is an algorithm called fully connected in fully connected layers to obtain final output images called classification.

**TABLE 3.** Similarities in the first and second classifications for the time period in Fig. 3 using the first CNN model. STD = 0.183, MSE = 0.035.

Day, May, 2003	First classification	Second classification
1	0.9937	0.0063
2	0.9740	0.0260
3	0.9992	0.0008
4	0.9993	0.0007
5	0.9997	0.0003
6	0.9992	0.0008
7	0.9682	0.0318
8	0.9904	0.0096
9	0.9720	0.0280
10	0.9785	0.0215
11	0.9993	0.0007
12	0.9998	0.0002
<b>13</b>	<b>0.4292</b>	0.5708
14	0.9998	0.0002
15	0.9999	0.0001
16	0.9989	0.0011
17	0.9917	0.0083
18	0.8137	0.1863
19	0.9800	0.0200
20	0.9969	0.0031
21	0.8999	0.1001
22	0.9989	0.0011
23	0.7999	0.2001
24	0.8349	0.1651

**IV. TOTAL ELECTRON CONTENT MAP PROCESSING USING CONVOLUTIONAL NEURAL NETWORKS**

In this section, the procedure of creating TEC maps using two CNN models is introduced as follows:

(1) The TEC map in Fig. 1 serves as a training image to create the CNN model called the first CNN model for detection of any TEC precursor of the Chi-Chi earthquake. The TEC map in Fig. 3 serves as a training image for the creation of another CNN model called the second CNN model for the detection of any TEC precursor of the earthquake on May 15, 2003 (TST). The first CNN model is used to verify the accuracy of the second CNN model and the second CNN model is used to verify the accuracy of the first CNN model.

(2) After two TEC maps are split from Fig. 1 and 3, 24 images from each TEC map—which are images obtained daily images—are used as training images to create two CNN models. The training images are used as inputs with two classifications to identify the TEC precursors of larger earthquakes. The 24 daily images belong to two classifications. The first classification is identified without earthquake-associated TEC anomalies. The second classification is identified with earthquake-associated TEC anomalies, namely

TEC precursors of earthquakes, which have been identified in the studies of Lin [36] and Liu *et al.* [41] in the daily images obtained on September 17, 18, and 20. Therefore, two classifications exist, and this research uses these image classifications.

(3) Splitting images causes wedge effects, which is a type of artificial image processing errors. In these split images used as inputs, a low pass filter called a Butterworth filter [10] is applied to reduce wedge effects for the split images in vertical and horizontal directions before the convolutional layers in the first hidden layer as described. The Butterworth filter has been identified as a suitable filter for TEC data [12], [67].

(4) For both CNN models, the training epoch is set as 2000 [47], and the learning rate is adaptive at 0 to 1, with an increment of 0.01. The batch size is required to reduce the computing time. The batch size is equal to 3. For the backpropagation algorithm, the initial weights and the initial biases were set to random variables [49], and feature scaling was then performed to ensure that these variables would be in the range from 0 and 1 [11] due to the range of the sigmoid function being 0–1 as described.



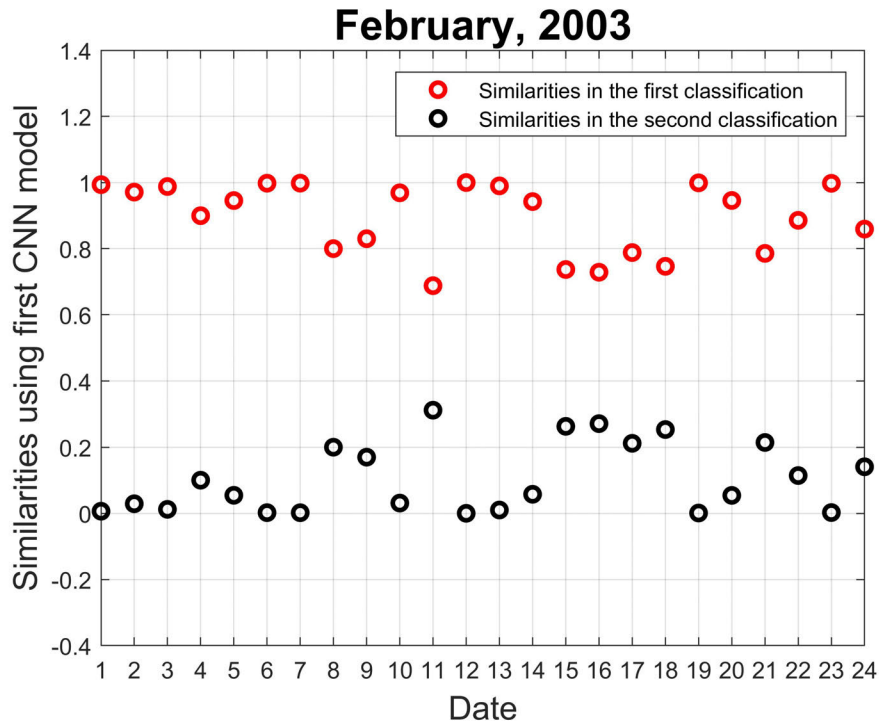


FIGURE 7. Visual presentation of Table 2.

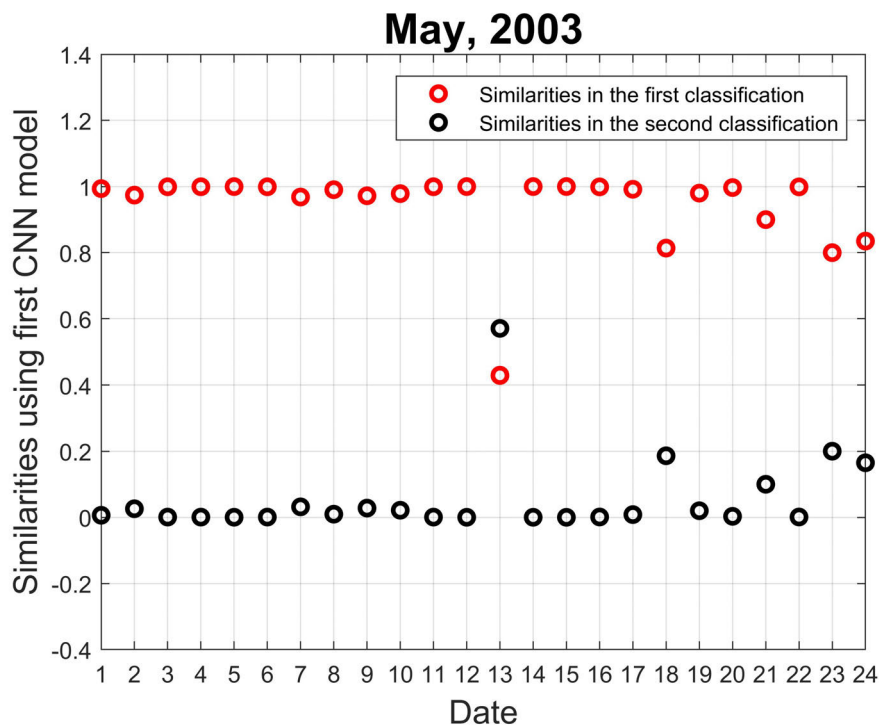


FIGURE 8. Visual presentation of Table 3.

Batch normalization is simultaneously performed as already described. The Levenberg–Marquardt algorithm is applied to obtain optimum weights and biases because it is superior to

other error back propagation algorithms for irregular and split image patterns [8], [38]. The best learning rates of the first and second CNN models are 0.25 and 0.19, respectively.

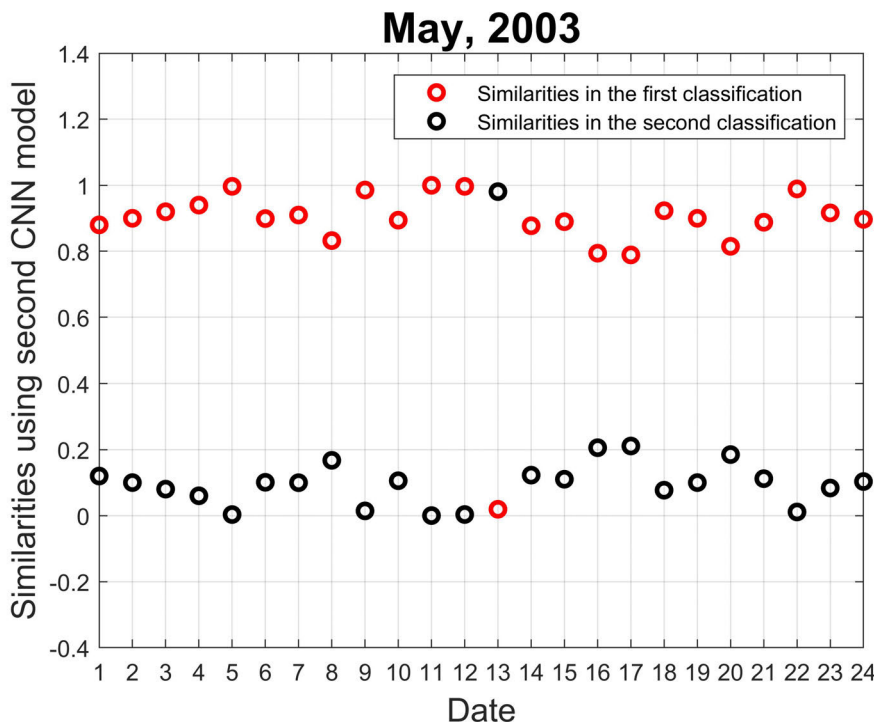


FIGURE 9. Visual presentation of Table 4.

(5) A final output is defined as a similarity belonging to a classification [26]. After normalization with feature scaling, this similarity is in the range between 0 and 1. If the value is equal to 1, then the respective classification is correct, and the daily TEC image is a complete TEC precursor. If the value is equal to 0, then its exact classification is an alternative classification, and the daily TEC image is not a TEC precursor. However, this describes perfect classification. In a real situation, daily TEC images cannot represent a complete TEC precursor. Therefore, the similarity value is between 0 and 1, and a threshold of similarities should be reasonably determined.

If the value is close to 1, more information on the TEC precursor is present in the daily TEC image. If the value is close to 0, then less information on the TEC precursor is present in the daily TEC image. In this study, a similarity  $0 \leq \text{similarity} < 0.5$  is defined as the first classification without information on the TEC precursor, and a similarity  $0.5 < \text{similarity} \leq 1$  is defined as the second classification with information on the TEC precursor. Therefore, two classifications of similarities are used as a new proposal. The flowchart of the procedure for creating a CNN model is shown in Fig. 5.

The source codes of the program set used for the CNN in this study, which have future development meaning reliability by the author according to the research objective, are obtained from <https://github.com/rasmusbergpalm/DeepLearnToolbox>.

V. RESULTS

Table 1 provides the results of the inside tests for the time period in Fig. 1 using the first CNN model to verify the

accuracy and reliability of this model’s prediction of TEC precursors for earthquakes with the magnitude ( $M_w$ )  $\geq 5.0$ . Fig. 6 depicts the visual presentation of Table 1. The similarities on September 17, 18, and 20 belong to the second classification. The results of the outside tests for the time period in Fig. 2 using the first CNN model are for the prediction of TEC precursors with the magnitude ( $M_w$ )  $\geq 5.0$  shown in Table 2. Fig. 7 depicts the visual presentation of Table.2. Their similarities belong to the first classification. No earthquakes with the magnitude ( $M_w$ )  $\geq 5.0$  occurred in this time period. Therefore, no TEC precursors are found. Table 3 shows the results of the outside tests for the time period in Fig. 3 using the first CNN model for the prediction of TEC precursors with the magnitude ( $M_w$ )  $\geq 5.0$ . Fig. 8 depicts the visual presentation of Table.3.

The similarity on May 13, 2003, belongs to the second classification. Table 4 shows the results of the inside tests for the time period in Fig. 3 using the second CNN model to verify the model’s accuracy and reliability for the prediction of TEC precursors of earthquakes with the magnitude ( $M_w$ )  $\geq 5.0$ . Fig. 9 depicts the visual presentation of Table.4. Table 5 shows the results of the outside tests for the time period in Fig. 1 using the second CNN model for the prediction of TEC precursors with the magnitude ( $M_w$ )  $\geq 5.0$ . Fig. 10 depicts the visual presentation of Table.5. The similarities on September 17, 18, and 20 belong to the second classification. Table 6 shows the results of the outside tests for the time period in Fig. 2 using the second CNN model for prediction of TEC precursors with the magnitude ( $M_w$ )  $\geq 5.0$ . Fig. 11 depicts the visual presentation of Table.6. Their similarities belong to the first classification because no TEC

**TABLE 4.** Similarities in the first and second classifications for the time period in Fig. 3 using the second CNN model. STD = 0.123, MSE = 0.029.

Day, May, 2003	First classification	Second classification
1	0.8800	0.1200
2	0.8999	0.1001
3	0.9197	0.0803
4	0.9399	0.0601
5	0.9967	0.0033
6	0.8990	0.1010
7	0.9098	0.0998
8	0.8324	0.1676
9	0.9856	0.0144
10	0.8942	0.1058
11	0.9998	0.0002
12	0.9966	0.0034
<b>13</b>	<b>0.0193</b>	<b>0.9807</b>
14	0.8773	0.1227
15	0.8897	0.1103
16	0.7942	0.2058
17	0.7890	0.2110
18	0.9229	0.0771
19	0.8999	0.1001
20	0.8150	0.1850
21	0.8880	0.1120
22	0.9889	0.0111
23	0.9163	0.0837
24	0.8967	0.1033

precursors occur due to the absence of earthquakes with the magnitude ( $M_w$ )  $\geq 5.0$  in this time period. The standard deviation (STD) and mean square error (MSE) are used as statistical approaches to evaluate the verified and prediction accuracy of the two CNN models for their reliable application [48], [38].

To verify the accuracy and reliability of the first CNN Model, the STD and MSE are 0.012 and 0.014, respectively, for the time period in Fig. 1 (Table 1). For the prediction accuracy and reliability of this CNN model, the STD and MSE are 0.162 and 0.026, respectively, for the time period in Fig. 2 (Table 2). For the prediction accuracy and reliability of this CNN model, the STD and MSE are 0.183 and 0.035, respectively, for the time period in Fig. 3 (Table 3). To verify the accuracy and reliability of the second CNN Model, the STD and MSE are 0.123 and 0.029, respectively for the time period in Fig. 3 (Table 4). For the prediction accuracy and reliability of this CNN model, the STD and MSE are 0.313 and 0.098, respectively for the time period in Fig. 1 (Table 5). For the prediction accuracy and reliability of this CNN model, the STD and MSE are 0.271 and 0.074, respectively for the time period in Fig. 2 (Table 6). Therefore, from previous

statements, the two CNN models are used to verify the accuracies of each other.

## VI. DISCUSSION

Through statistical analysis, researchers such as Liu *et al.* [43] found that most of the ionospheric anomalies were exhibited a few days prior to larger earthquakes. The ionospheric anomalies exhibiting a sparse TEC were detected 5 days prior to large earthquakes with the magnitude ( $M_w$ )  $\geq 5.0$ . TEC precursors termed temporal TEC multi-precursors (TTMPs) [72] related to the Chi-Chi earthquake on September 21, 1999, were detectable on the 1st, 3rd, and 4th days prior to the Chi-Chi earthquake, that is, on September 17, 18, and 20, 1999, respectively [41]. Therefore, the similarities on September 17, 18, and 20, 1999, belong to the second classification of TEC precursors, and other daily images belong to the first classification. Such TEC precursors are TTMPs, which differ from the STMPs in the study of Lin *et al.* [39]. These results are consistent with those of Lin [36] and Liu *et al.* [41]. Lin [36] examined TEC data using principal component analysis (also called Karhunen–Loève transform) to detect the Chi-Chi earthquake's TEC precursors on September 17, 18,

**TABLE 5.** Similarities in the first and second classifications for the time period in Fig. 1 using the second CNN model. STD = 0.313, MSE = 0.098.

Day, September, 1999	First classification	Second classification
1	0.6700	0.3300
2	0.5800	0.4200
3	0.7900	0.2100
4	0.8200	0.1800
5	0.7845	0.2155
6	0.6800	0.3200
7	0.7825	0.2175
8	0.8700	0.1300
9	0.6700	0.3300
10	0.5745	0.4255
11	0.6400	0.3600
12	0.7910	0.2090
13	0.7997	0.2003
14	0.6770	0.3230
15	0.6998	0.3002
16	0.6942	0.3058
<b>17</b>	<b>0.4343</b>	<b>0.5657</b>
<b>18</b>	<b>0.4900</b>	<b>0.5100</b>
19	0.6999	0.3001
<b>20</b>	<b>0.4990</b>	<b>0.5010</b>
21	0.6885	0.3115
22	0.7889	0.2111
23	0.6953	0.3047
24	0.6757	0.3243

and 20, 1999. A similarity on May 13, 2003, belongs to the second classification because a TEC precursor should be associated with the earthquake on May 15, 2003 (TST) with the magnitude ( $M_w$ ) = 5.52. This TEC precursor was detectable 2 days prior to this earthquake. The reliable application of a low pass filter is therefore discussed. Three split daily images on September 17, 18, and 20 from Fig. 1 without a low pass filter and another 21 split daily images from Fig. 1 as inputs with a Butterworth filter are used in the second CNN model. The three similarities on September 17, 18, and 20 are shown in **Table 7**. The similarity of split daily images from September 18 belongs to the first classification, which is considered a non-TEC precursor in this day. The wedge effects may have caused an error in the identification of the TEC precursor, indicating that a low pass filter must be used. This represents a major improvement that is advantageous in this study.

The low STD and MSE values confirm the reliability of both CNN models by using them to verify each other's accuracies. The prediction errors of both CNN models are relatively small, and the prediction errors of the outside tests are slightly larger than those of the inside tests from Table 1 to

Table 6 (Fig.6-11). Therefore, both CNN models are suitable and reliable for the prediction of TEC precursor prior to large earthquakes. Specifically, factors such as the kp index value, as mentioned, do not require consideration during the training of the CNN model. Furthermore, using a low pass filter belonged to the preprocessing was already considered when training the CNN model. Unlike in other studies, the TEC precursors do not require distinguishing from other TEC anomalies in this study. Thus, the features of CNN models are a prominent advantage of this study. The only concern is the accuracy for the prediction of the TEC precursors. Only a few TEC maps are used as the training images. These training images, from a short-time period, overcame the nonstationary influence of TEC seasonal variations, which indicates that the two CNN models are valuable. This study also confirms that the TEC precursor for earthquakes with the magnitude ( $M_w$ ) < 5.0 is not induced in Taiwan. Therefore, the two models achieve the goal of this study, fitting with the results of the study by Liu *et al.* [43]. In this study, the two hidden layers were used. Future research should develop a better and more suitable AI algorithm with suitable numbers of hidden layers (e.g., support vector machine and extreme machine learning)

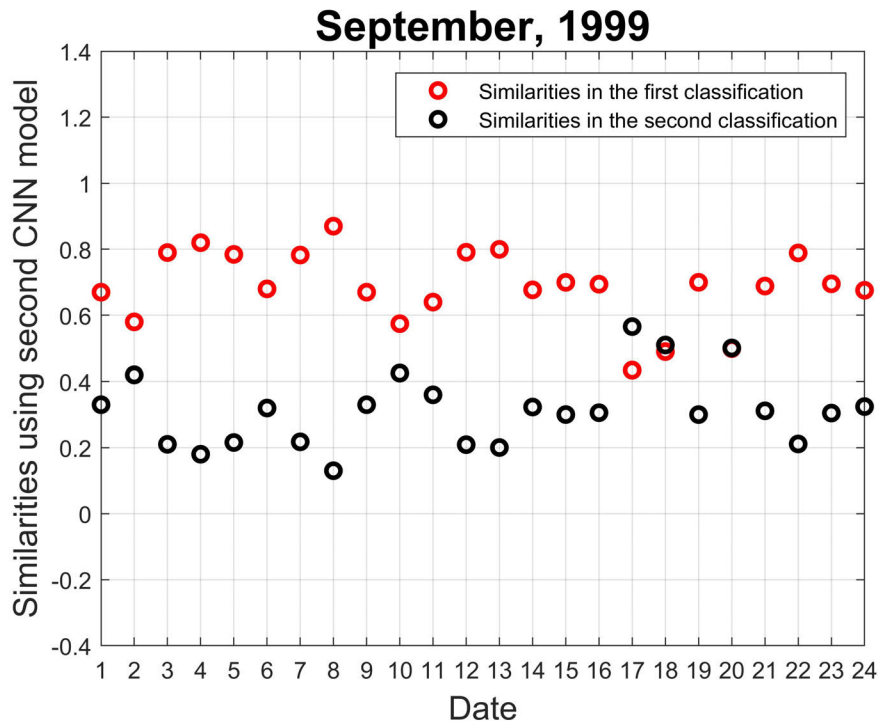


FIGURE 10. Visual presentation of Table 5.

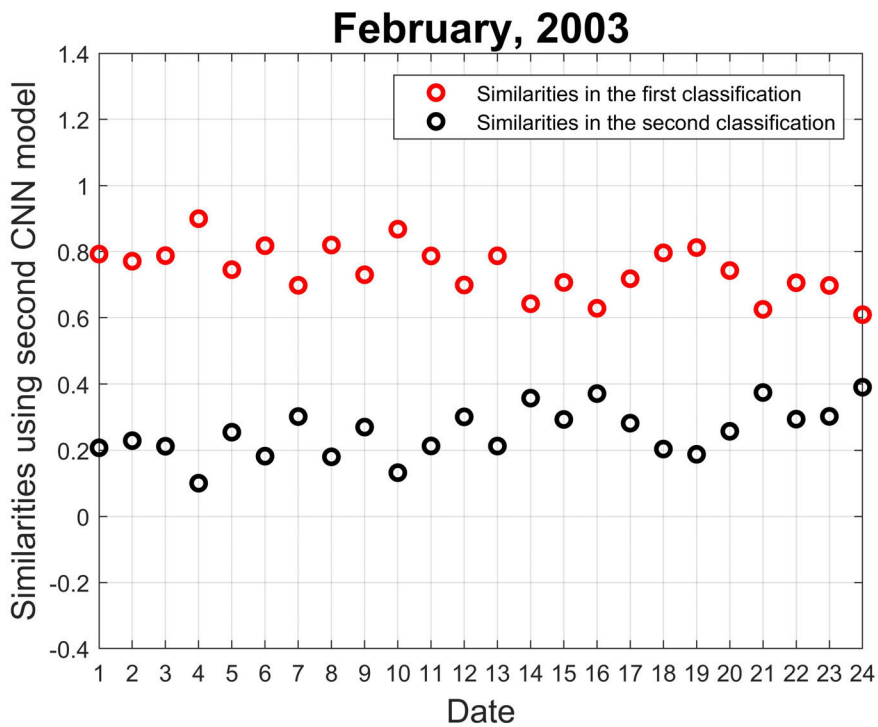


FIGURE 11. Visual presentation of Table 6.

with a better and more suitable error back propagation algorithm (e.g., scaled conjugate gradient algorithm) to realize an optimized AI mode for this topic. The CNN model used in

this study is a passive model, meaning the framework is not determined using training images. Therefore, for an optimal active CNN model, as per the concept of Lin *et al.* [38],

**TABLE 6.** Similarities in the first and second classifications for the time period in Fig. 2 using the second CNN model. STD = 0.271, MSE = 0.074.

Day, February, 2003	First classification	Second classification
1	0.7926	0.2074
2	0.7710	0.2290
3	0.7879	0.2121
4	0.8997	0.1003
5	0.7454	0.2546
6	0.8179	0.1821
7	0.6981	0.3019
8	0.8199	0.1801
9	0.7300	0.2700
10	0.8679	0.1321
11	0.7870	0.2130
12	0.6990	0.3010
13	0.7873	0.2127
14	0.6423	0.3577
15	0.7068	0.2932
16	0.6286	0.3714
17	0.7180	0.2820
18	0.7964	0.2036
19	0.8123	0.1877
20	0.7427	0.2573
21	0.6253	0.3747
22	0.7059	0.2941
23	0.6976	0.3024
24	0.6093	0.3907

**TABLE 7.** Three similarities on September 17, 18, and 20 from Fig. 1 using the second CNN model.

Day, September, 1999	First classification	Second classification
<b>17</b>	<b>0.4921</b>	<b>0.5077</b>
<b>18</b>	<b>0.5201</b>	<b>0.4799</b>
<b>20</b>	<b>0.4719</b>	<b>0.5281</b>

the framework of a CNN model can be determined using fewer training images to reduce costs and computing times for image processing.

Regarding chemical, physical and mechanical principles and reasons to cause the ionospheric TEC precursors observed before earthquakes have been a prominent area of research in the field of seismoionospheric Solid Earth–Atmosphere coupling [17], [51], [23], [53], [30], [19], [29], [59]. Freund [17] reported ionosphere precursors by using p-type semiconductors; the earth dipole field of earthquakes; magnetic field anomalies; and positive holes due to crackled, sparkled, and glowed igneous and metamorphic rocks before large earthquakes. Hegai *et al.* [23] found the ionospheric precursors by the internal atmospheric

gravity waves and enhancements of the vertical electric field generated before strong earthquakes. Pulnits [51] detected the ionospheric precursors of earthquakes caused by anomalous electric fields involving in ionospheric variations. Pulnits and Ouzounov [53] examined ionospheric precursors by using radon gases with the Lithosphere–Atmosphere–Ionosphere Coupling model. Fu *et al.* [19] detected ionospheric precursors by radon gases before the 2016 M 6.6 Meinong earthquake. Kamogawa and Kakinami [30] detected TEC enhancement as a precursor caused by a tsunami-genic ionospheric hole after the coseismic acoustic waves. Tachema and Nadji [59] confirmed the TEC precursors caused by the electromagnetic for the 2008 Oran earthquake, Algeria.



Significant TEC decreases because TTMPs related to the Chi-Chi earthquake were caused by an electric field [41]. The cause of the TEC precursor on May 13, 2003, before the earthquake that occurred on May 15, 2003, will be an argument with any corresponding study, which is to be referred. A similarity = 0.5 was another argument to cause the classifications become meaningless. Finally, the results of the study are consistent with those of Lin [36] and Liu *et al.* [41] related to the Chi-Chi earthquake. Therefore, the application of this study is reliable.

## VII. CONCLUSION

The TEC maps used in this study are from the Chung-Li station, one of the ground network stations of the CWB ionospheric observatory in Taiwan. The TEC maps examined at this station reflect the seismic activity of Taiwan called Chung-Li Ionosonde. Therefore, daily TEC images obtained through TEC map splitting were used as training images for two CNN models encompassing three time periods: September 1 to 24, 1999, February 1 to 24, 2003, and May 1 to 24, 2003 (TST). The aim was to verify the accuracy and rationality of the research results using CNN models from this study. A Butterworth filter was used to reduce wedge effects, a type of artificial image-processing error, and to obtain better data on TEC precursors. Statistical analysis was not attempted. Similarities larger than 0.5 were defined as TEC precursors of earthquakes. The TTMPs of the Chi-Chi earthquake on September 21, 1999, were detectable on the 1st, 3rd, and 4th days prior to the Chi-Chi earthquake, that is, Karhunen-Loève Trans form. These results are consistent with those of Lin [36] and Liu *et al.* [41].

A TEC precursor on May 13, 2003 (TST) was detectable two days prior to an earthquake on May 15, 2003 (TST) with the magnitude ( $M_w = 5.52$ ). The low STD and MSE values confirm the reliability of the two CNN models. The TTMPs related to the Chi-Chi earthquake were caused by an electric field. The cause of the TEC precursor on May 13, 2003, prior to the earthquake on May 15, 2003, was an argument without any corresponding study to be compared.

## DATA AVAILABILITY

The TEC data can be acquired from the Central Weather Bureau of Taiwan (CWB).

The program source code of this study is from the source web <https://github.com/rasmusbergpalm/DeepLearnToolbox>

## ACKNOWLEDGMENT

The authors are grateful to Central Weather Bureau of Taiwan (CWB) for the useful references data.

## COMPETING INTERESTS

The authors declare that they have no competing interests.

## REFERENCES

- [1] J. Ádám and K. P. Schwarz, *Vistas for Geodesy in the New Millennium*. Berlin, Germany: Springer-Verlag, 2001, p. 622, doi: [10.1007/978-3-662-04709-5](https://doi.org/10.1007/978-3-662-04709-5).
- [2] E. L. Afraimovich and E. I. Astafyeva, "TEC anomalies—Local TEC changes prior to Earth quakes or TEC response to solar and geomagnetic activity changes?" *Earth, Planets Space*, vol. 60, no. 9, pp. 961–966, Sep. 2008, doi: [10.1186/BF03352851](https://doi.org/10.1186/BF03352851).
- [3] H. H. Aghdam and E. J. Heravi *Guide to Convolutional Neural Networks*. Berlin, Germany: Springer, 2017, p. 282, doi: [10.1007/978-3-319-57550-6](https://doi.org/10.1007/978-3-319-57550-6).
- [4] B. A. S. Aji, T. H. Liong, and B. Muslim, "Detection precursor of sumatra Earthquake based on ionospheric total electron content anomalies using N-model artificial neural network," in *Proc. Int. Conf. Adv. Comput. Sci. Inf. Syst. (ICACIS)*, vol. 17738122, Oct. 2017, pp. 1–4, doi: [10.1109/ICACIS.2017.8355045](https://doi.org/10.1109/ICACIS.2017.8355045).
- [5] M. Akhoondzadeh, "An adaptive network-based fuzzy inference system for the detection of thermal and TEC anomalies around the time of the varzeghan, Iran, (Mw=6.4) earthquake of 11 August 2012," *Adv. Space Res.*, vol. 52, no. 5, pp. 837–852, Sep. 2013, doi: [10.1016/j.asr.2013.05.024](https://doi.org/10.1016/j.asr.2013.05.024).
- [6] M. Akhoondzadeh, "Thermal and TEC anomalies detection using an intelligent hybrid system around the time of the saravan, iran, (Mw=7.7) earthquake of 16 April 2013," *Adv. Space Res.*, vol. 53, no. 4, pp. 647–655, Feb. 2014, doi: [10.1016/j.asr.2013.12.017](https://doi.org/10.1016/j.asr.2013.12.017).
- [7] M. Akhoondzadeh, A. De Santis, D. Marchetti, A. Piscini, and S. Jin, "Anomalous seismo-LAI variations potentially associated with the 2017 mw = 7.3 Sarpol-e zahab (Iran) Earthquake from swarm satellites, GPS-TEC and climatological data," *Adv. Space Res.*, vol. 64, no. 1, pp. 143–158, Jul. 2019, doi: [10.1016/j.asr.2019.03.020](https://doi.org/10.1016/j.asr.2019.03.020).
- [8] C. Alippi, *Intelligence for Embedded Systems: A Methodological Approach*. Cham, Switzerland: Springer, 2014.
- [9] F. W. G. White and M. Geddes, "The antractic zone of maximum auroral frequency," *J. Geophys. Res.*, vol. 44, no. 4, p. 367, 1939, doi: [10.1029/TE044i004p00367](https://doi.org/10.1029/TE044i004p00367).
- [10] G. Bianchi and R. Sorrentino, *Electronic Filter Simulation & Design*. New York, NY, USA: McGraw-Hill, 2007, p. 606.
- [11] L. Bo, L. Wang, and L. Jiao, "Feature scaling for kernel Fisher discriminant analysis using leave-one-out cross validation," *Neural Comput.*, vol. 18, no. 4, pp. 961–978, Apr. 2006, doi: [10.1162/neco.2006.18.4.961](https://doi.org/10.1162/neco.2006.18.4.961).
- [12] E. Chandrasekhar, S. S. Prabhudesai, G. K. Seemala, and N. Shenvi, "Multifractal detrended fluctuation analysis of ionospheric total electron content data during solar minimum and maximum," *J. Atmos. Solar-Terrestrial Phys.*, vol. 149, pp. 31–39, Nov. 2016, doi: [10.1016/j.jastp.2016.09.007](https://doi.org/10.1016/j.jastp.2016.09.007).
- [13] S. Chatterjee, S. K. Chakraborty, B. Veenadhari, and S. Banola, "A study on ionospheric scintillation near the EIA crest in relation to equatorial electrodynamics," *J. Geophys. Res., Space Phys.*, vol. 119, no. 2, pp. 1250–1261, Feb. 2014, doi: [10.1002/2013JA019466](https://doi.org/10.1002/2013JA019466).
- [14] Y.-J. Chuo, "Variations of scale height at F-region peak based on ionosonde measurements during solar maximum over the crest of equatorial ionization anomaly region," *Sci. World J.*, vol. 2014, Aug. 2014, Art. no. 397402, doi: [10.1155/2014/397402](https://doi.org/10.1155/2014/397402).
- [15] Y. Chu, J. Fei, and S. Hou, "Adaptive global sliding-mode control for dynamic systems using double hidden layer recurrent neural network structure," *IEEE Trans. Neural Netw. Learn. Syst.*, vol. 31, no. 4, pp. 1297–1309, Feb. 2020, doi: [10.1109/TNNLS.2019.2919676](https://doi.org/10.1109/TNNLS.2019.2919676).
- [16] *Middle Atmosphere Program: Handbook for Map, vol. 27, Scientific Committee on Solar-Terrestrial Physics (SCOSTEP) Secretariat*, University of Illinois, Urbana, IL, USA, 1989.
- [17] F. T. Freund, "Rocks that crackle and sparkle and glow strange pre-Earthquake phenomena," *J. Sci. Explor.*, vol. 17, no. 1, pp. 37–71, 2003.
- [18] J. Fei and Y. Chu, "Double hidden layer output feedback neural adaptive global sliding mode control of active power filter," *IEEE Trans. Power Electron.*, vol. 35, no. 3, pp. 3069–3084, Mar. 2020, doi: [10.1109/tpel.2019.2925154](https://doi.org/10.1109/tpel.2019.2925154).
- [19] C.-C. Fu, V. Walia, T. F. Yang, L.-C. Lee, T.-K. Liu, C.-H. Chen, A. Kumar, S.-J. Lin, T.-H. Lai, and K.-L. Wen, "Preseismic anomalies in soil-gas radon associated with 2016 m 6.6 meinong Earthquake, southern taiwan," *Terr., Atmos. Ocean. Sci.*, vol. 28, no. 5, pp. 787–798, 2017, doi: [10.3319/TAO.2017.03.22.01](https://doi.org/10.3319/TAO.2017.03.22.01).
- [20] F. Sabzehee, S. Farzaneh, M. A. Sharifi, and M. Akhoondzadeh, "TEC regional modeling and prediction using ANN method and single frequency receiver over IRAN," *Ann. Geophys.*, vol. 61, no. 1, p. GM103, 2018. [Online]. Available: <https://www.annalsofgeophysics.eu/index.php/annals/article/view/7297>, doi: [10.4401/ag-7297](https://doi.org/10.4401/ag-7297).

- [21] M. Hayakawa, *Earthquake Prediction with Radio Techniques*. Hoboken, NJ, USA: Wiley, 2016, p. 304, doi: [10.1002/9781118770368](https://doi.org/10.1002/9781118770368).
- [22] M. A. Hanzaei, "Kalman filter and Neural Network methods for detecting irregular variations of TEC around the time of powerful Mexico (Mw=8.2) earthquake of Sep. 08, 2017," *J. Earth Space Phys.*, vol. 44, no. 4, pp. 87–97, 2018, doi: [10.22059/jesphys.2018.258251.1007007](https://doi.org/10.22059/jesphys.2018.258251.1007007).
- [23] V. V. Hegai, V. P. Kim, and J. Y. Liu, "The ionospheric effect of atmospheric gravity waves excited prior to strong earthquake," *Adv. Space Res.*, vol. 37, no. 4, pp. 653–659, Jan. 2006, doi: [10.1016/j.asr.2004.12.049](https://doi.org/10.1016/j.asr.2004.12.049).
- [24] G.-B. Huang, "Learning capability and storage capacity of two-hidden-layer feedforward networks," *IEEE Trans. Neural Netw.*, vol. 14, no. 2, pp. 274–281, Mar. 2003, doi: [10.1109/TNN.2003.809401](https://doi.org/10.1109/TNN.2003.809401).
- [25] Y.-Y. Ho, H.-K. Jhuang, L.-C. Lee, and J.-Y. Liu, "Ionospheric density and velocity anomalies before  $m > 6.5$  earthquakes observed by DEMETER satellite," *J. Asian Earth Sci.*, vol. 166, pp. 210–222, Oct. 2018, doi: [10.1016/j.jseaes.2018.07.022](https://doi.org/10.1016/j.jseaes.2018.07.022).
- [26] D. R. Hush and B. G. Horne, "Progress in supervised neural networks," *IEEE Signal Process. Mag.*, vol. 10, no. 1, pp. 8–39, Jan. 1993, doi: [10.1109/79.180705](https://doi.org/10.1109/79.180705).
- [27] S. Inyurt and A. Sekertekin, "Modeling and predicting seasonal ionospheric variations in turkey using artificial neural network (ANN)," *Astrophys. Space Sci.*, vol. 364, no. 4, Apr. 2019, doi: [10.1007/s10509-019-3545-9](https://doi.org/10.1007/s10509-019-3545-9).
- [28] C. Ji and D. Psaltis, "Capacity of two-layer feedforward neural networks with binary weights," *IEEE Trans. Inf. Theory*, vol. 44, no. 1, pp. 256–268, 1998, doi: [10.1109/18.651033](https://doi.org/10.1109/18.651033).
- [29] S. Jin, R. Jin, and X. Liu, *GNSS Atmospheric Seismology: Theory, Observations and Modeling*. Singapore: Springer, 2019, p.315, doi: [10.1007/978-981-10-3178-6\\_9](https://doi.org/10.1007/978-981-10-3178-6_9).
- [30] M. Kamogawa and Y. Kakinami, "Is an ionospheric electron enhancement preceding the 2011 tohoku-oki earthquake a precursor?: Did TEC enhance before Tohoku Eq?" *J. Geophys. Res., Space Phys.*, vol. 118, no. 4, pp. 1751–1754, Apr. 2013, doi: [10.1002/jgra.50118](https://doi.org/10.1002/jgra.50118).
- [31] H. Kim, J. Son, and J. Lee, "A high-speed sliding-mode observer for the sensorless speed control of a PMSM," *IEEE Trans. Ind. Electron.*, vol. 58, no. 9, pp. 4069–4077, Sep. 2011, doi: [10.1109/TIE.2010.2098357](https://doi.org/10.1109/TIE.2010.2098357).
- [32] M. V. Klimenko, V. V. Klimenko, I. E. Zakharenkova, and S. A. Pulnits, "Variations of equatorial electrojet as possible seismo-ionospheric precursor at the occurrence of TEC anomalies before strong Earthquake," *Adv. Space Res.*, vol. 49, no. 3, pp. 509–517, Feb. 2012, doi: [10.1016/j.asr.2011.10.017](https://doi.org/10.1016/j.asr.2011.10.017).
- [33] D. Li, J. Wang, J. Xu, and X. Fang, "Densely feature fusion based on convolutional neural networks for motor imagery EEG classification," *IEEE Access*, vol. 7, pp. 132720–132730, 2019, doi: [10.1109/ACCESS.2019.2941867](https://doi.org/10.1109/ACCESS.2019.2941867).
- [34] W.-H. Li, C.-H. Lee, M.-H. Ma, P. J. Huang, and S. Y. Wu, "Fault dynamics of the 1999 chi-chi earthquake: Clues from nanometric geochemical analysis of fault gouges," *Sci. Rep.*, vol. 9, no. 1, Dec. 2019, Art. no. 5683, doi: [10.1038/s41598-019-42028-w](https://doi.org/10.1038/s41598-019-42028-w).
- [35] G. Liang, H. Hong, W. Xie, and L. Zheng, "Combining convolutional neural network with recursive neural network for blood cell image classification," *IEEE Access*, vol. 6, pp. 36188–36197, 2018, doi: [10.1109/ACCESS.2018.2846685](https://doi.org/10.1109/ACCESS.2018.2846685).
- [36] J. W. Lin, "Ionospheric total electron content (TEC) anomalies associated with Earthquakes through Karhunen-Loève transform (KLT), terrestrial," *Atmos. Ocean. Sci. J.*, vol. 21, no. 2, pp. 253–265, 2010. [Online]. Available: <http://tao.cgu.org.tw/index.php/articles/archive/geophysics/item/903>, doi: [10.3319/TAO.2009.06.11.01\(T\)](https://doi.org/10.3319/TAO.2009.06.11.01(T)).
- [37] J.-W. Lin, "Taiwan' chi-chi earthquake precursor detection using non-linear principal component analysis to multi-channel total electron content records," *J. Earth Sci.*, vol. 24, no. 2, pp. 244–253, Apr. 2013, doi: [10.1007/s12583-013-0325-2](https://doi.org/10.1007/s12583-013-0325-2).
- [38] J.-W. Lin, C.-T. Chao, and J.-S. Chiou, "Determining neuronal number in each hidden layer using earthquake catalogues as training data in training an embedded back propagation neural network for predicting earthquake magnitude," *IEEE Access*, vol. 6, pp. 52582–52597, 2018, doi: [10.1109/ACCESS.2018.2870189](https://doi.org/10.1109/ACCESS.2018.2870189).
- [39] J.-W. Lin, J.-S. Chiou, and C.-T. Chao, "Detecting all possible ionospheric precursors by kernel-based two-dimensional principal component analysis," *IEEE Access*, vol. 7, pp. 53650–53666, 2019, doi: [10.1109/ACCESS.2019.2912564](https://doi.org/10.1109/ACCESS.2019.2912564).
- [40] Z. Lin, S. Mu, F. Huang, K. A. Mateen, M. Wang, W. Gao, and J. Jia, "A unified matrix-based convolutional neural network for fine-grained image classification of wheat leaf diseases," *IEEE Access*, vol. 7, pp. 11570–11590, 2019, doi: [10.1109/ACCESS.2019.2891739](https://doi.org/10.1109/ACCESS.2019.2891739).
- [41] J. Y. Liu, Y. C. Chuo, and H. F. Tsai, "Variations of ionospheric total electron content during the Chi-Chi Earthquake," *Geophys. Res. Lett.*, vol. 28, no. 7, pp. 1383–1386, 2001, doi: [10.1029/2000GL012511](https://doi.org/10.1029/2000GL012511).
- [42] J. Y. Liu, Y. I. Chen, H. K. Jhuang, and Y. H. Lin, "Ionospheric foF<sub>2</sub> and TEC anomalous days associated with M 5.0 Earthquakes in taiwan during 1997-1999, terrestrial," *Atmos. Ocean. Sci.*, vol. 15, no. 3, pp. 371–383, 2004, doi: [10.3319/TAO.2004.15.3.371\(EP\)](https://doi.org/10.3319/TAO.2004.15.3.371(EP)).
- [43] J. Y. Liu, C. H. Chen, Y. I. Chen, H. Y. Yen, K. Hattori, and K. Yumoto, "Seismo-geomagnetic anomalies and M 5.0 earthquakes observed in taiwan during 1988–2001," *Phys. Chem. Earth*, vol. 31, nos. 4–9, pp. 215–222, Jan. 2006, doi: [10.1016/j.pce.2006.02.009](https://doi.org/10.1016/j.pce.2006.02.009).
- [44] J. Liu, X. Zhang, V. Novikov, and X. Shen, "Variations of ionospheric plasma at different altitudes before the 2005 sumatra indonesia m s 7.2 Earthquake," *J. Geophys. Res., Space Phys.*, vol. 121, no. 9, pp. 9179–9187, Sep. 2016, doi: [10.1002/2016JA022758](https://doi.org/10.1002/2016JA022758).
- [45] P. I. Nenovski, M. Pezzopane, L. Ciraolo, M. Vellante, U. Villante, and M. De Lauretis, "Local changes in the total electron content immediately before the 2009 abruzzo Earthquake," *Adv. Space Res.*, vol. 55, no. 1, pp. 243–258, Jan. 2015, doi: [10.1016/j.asr.2014.09.029](https://doi.org/10.1016/j.asr.2014.09.029).
- [46] M. Nishihashi, K. Hattori, and K. Saroso, "Spatial distribution of ionospheric GPS-TEC and MnF<sub>2</sub> anomalies associated with the Chi-Chi Earthquake," *J. Sains Dirgantara*, vol. 7, no. 1, pp. 220–229, 2009.
- [47] S. Omatu, S. Rodriguez, G. Villarrubia, P. Faria, P. Sitek, and J. Prieto, "Distributed Computing and Artificial Intelligence," in *Proc. 14th Int. Conf. Berlin, Germany: Springer*, 2018, p. 344, doi: [10.1007/978-3-319-62410-5](https://doi.org/10.1007/978-3-319-62410-5).
- [48] E. Maleki and A. Zabihollah, "Modeling of shot-peening effects on the surface properties of a (TiB+TiC)/Ti–6Al–4 V composite employing artificial neural networks," *Materiali Tehnologije*, vol. 50, no. 6, pp. 851–860, Dec. 2016, doi: [10.17222/mit.2015.140](https://doi.org/10.17222/mit.2015.140).
- [49] D. Nguyen and B. Widrow, "Improving the learning speed of 2-layer neural networks by choosing initial values of the adaptive weights," in *Proc. IJCNN Int. Joint Conf. Neural Netw. Comput. Sci.*, 1990. [Online]. Available: <https://www.semanticscholar.org/paper/Improving-the-learning-speed-of-2-layer-neural-by-Nguyen-Widrow/fbe24a2d9598c620324e3bd51e2f817cd35e9c81>, doi: [10.1109/IJCNN.1990.137819](https://doi.org/10.1109/IJCNN.1990.137819).
- [50] T. Perol, M. Gharbi, and M. Denolle, "Convolutional neural network for Earthquake detection and location," *Sci. Adv.*, vol. 4, no. 2, Feb. 2018, Art. no. e1700578, doi: [10.1126/sciadv.1700578](https://doi.org/10.1126/sciadv.1700578).
- [51] S. A. Pulnits, "Ionospheric precursors of Earthquakes: Recent advances in theory and practical applications," *Terr. Atmos. Ocean. Sci.*, vol. 15, no. 3, pp. 413–435, 2004. [Online]. Available: <http://tao.cgu.org.tw/index.php/articles/archive/geophysics/item/529-2004153413ep>, doi: [10.3319/TAO.2004.15.3.413\(EP\)](https://doi.org/10.3319/TAO.2004.15.3.413(EP)).
- [52] S. Pulnits and K. Boyarchuk, *Ionospheric Precursors of Earthquakes*. Berlin, Germany: Springer-Verlag, 2005, p. 315, doi: [10.1007/b137616](https://doi.org/10.1007/b137616).
- [53] S. Pulnits and D. Ouzounov, "Lithosphere-atmosphere-ionosphere coupling (LAIC) model—An unified concept for Earthquake precursors validation," *J. Asian Earth Sci.*, vol. 41, nos. 4–5, pp. 371–382, Jun. 2011, doi: [10.1016/j.jseaes.2010.03.005](https://doi.org/10.1016/j.jseaes.2010.03.005).
- [54] I. Sacramento, M. Roisenberg, R. Exterkoetter, L. P. de Figueiredo, and B. Rodrigues, "Combined convolutional neural network for high frequency restoration in acoustic impedance images," in *Proc. Int. Joint Conf. Neural Netw. (IJCNN)*, Jul. 2018, pp. 1–4, doi: [10.1109/IJCNN.2018.8489672](https://doi.org/10.1109/IJCNN.2018.8489672).
- [55] *Plasma Physics, and Chemistry*, Cambridge, U.K.: Cambridge Univ. Press, 2020, p. 640, doi: [10.1017/CBO9780511635342](https://doi.org/10.1017/CBO9780511635342).
- [56] A. F. Somputa, N. T. Puspito, E. Joelianto, and K. Hattori, "Analysis of ionospheric precursor of Earthquake using GIM-TEC, kriging and neural network," *Asian J. Earth Sci.*, vol. 8, no. 2, pp. 32–44, Feb. 2015, doi: [10.3923/ajes.2015.32.44](https://doi.org/10.3923/ajes.2015.32.44).
- [57] M. Shah, M. A. Tariq, J. Ahmad, N. A. Naqvi, and S. Jin, "Seismo ionospheric anomalies before the 2007 M7.7 chile earthquake from GPS TEC and DEMETER," *J. Geodynamics*, vol. 127, pp. 42–51, Jun. 2019, doi: [10.1016/j.jog.2019.05.004](https://doi.org/10.1016/j.jog.2019.05.004).
- [58] R. Song, X. Zhang, C. Zhou, J. Liu, and J. He, "Predicting TEC in China based on the neural networks optimized by genetic algorithm," *Adv. Space Res.*, vol. 62, no. 4, pp. 745–759, Aug. 2018, doi: [10.1016/j.asr.2018.03.043](https://doi.org/10.1016/j.asr.2018.03.043).
- [59] A. Tachema and A. Nadjji, "Contribution of ionospheric TEC anomalies to detecting the seismic precursors related to the 2008 Oran-Algeria event," *Adv. Space Res.*, vol. 65, no. 11, pp. 2259–2572, Jun. 2020, doi: [10.1016/j.asr.2020.03.007](https://doi.org/10.1016/j.asr.2020.03.007).

- [60] N. Takahashi, M. Nagayoshi, S. Kawabata, and T. Nishi, "Stable patterns realized by a class of one-dimensional two-layer CNNs," *IEEE Trans. Circuits Syst. I, Reg. Papers*, vol. 55, no. 11, pp. 3607–3620, Dec. 2008, doi: [10.1109/TCSI.2008.925828](https://doi.org/10.1109/TCSI.2008.925828).
- [61] D. Tao, J. Cao, R. Battiston, L. Li, Y. Ma, W. Liu, Z. Zhima, L. Wang, and M. W. Dunlop, "Seismo-ionospheric anomalies in ionospheric TEC and plasma density before the 17 July 2006 M7.7 south of Java Earthquake," *Ann. Geophys.*, vol. 35, no. 3, pp. 589–598, Apr. 2017, doi: [10.5194/angeo-35-589-2017](https://doi.org/10.5194/angeo-35-589-2017).
- [62] J. N. Thomas, J. Huard, and F. Masci, "A statistical study of global ionospheric map total electron content changes prior to occurrences of  $m > 6.0$  earthquakes during 2000–2014," *J. Geophys. Res., Space Phys.*, vol. 122, no. 2, pp. 2151–2161, Feb. 2017, doi: [10.1002/2016JA023652](https://doi.org/10.1002/2016JA023652).
- [63] L. C. Tsai and W. H. Tsai, "Improvement of GPS/MET ionospheric profiling and validation using the Chung-Li Ionosonde measurements and the IRI model, terrestrial," *Atmos. Ocean. Sci.*, vol. 15, no. 4, pp. 589–607, 2004, doi: [10.3319/TAO.2004.15.4.589\(A\)](https://doi.org/10.3319/TAO.2004.15.4.589(A)).
- [64] Y. D. Wang, D. C. Pi, X. M. Zhang, and X. H. Shen, "Seismo-ionospheric precursory anomalies detection from DEMETER satellite data based on data mining," *Natural Hazards*, vol. 76, no. 2, pp. 823–837, Mar. 2015, doi: [10.1007/s11069-014-1519-3](https://doi.org/10.1007/s11069-014-1519-3).
- [65] C.-Y. Wang, C.-L. Su, K.-H. Wu, and Y.-H. Chu, "Cross spectral analysis of CODAR-SeaSonde echoes from sea surface and ionosphere at taiwan," *Int. J. Antennas Propag.*, vol. 2017, pp. 1–14, Oct. 2017, doi: [10.1155/2017/1756761](https://doi.org/10.1155/2017/1756761).
- [66] S. Wang, M. Roger, J. Sarrazin, and C. Lelandais-Perrault, "Hyperparameter optimization of Two-Hidden-Layer neural networks for power amplifiers behavioral modeling using genetic algorithms," *IEEE Microw. Wireless Compon. Lett.*, vol. 29, no. 12, pp. 802–805, Dec. 2019, doi: [10.1109/LMWC.2019.2950801](https://doi.org/10.1109/LMWC.2019.2950801).
- [67] Y. Wen and S. Jin, "Traveling ionospheric disturbances characteristics during the 2018 typhoon maria from GPS observations," *Remote Sens.*, vol. 12, no. 4, p. 746, Feb. 2020, doi: [10.3390/rs12040746](https://doi.org/10.3390/rs12040746).
- [68] M. J. Willis, C. Di Massimo, G. A. Montague, M. T. Tham, and A. J. Morris, "Artificial neural networks in process engineering," *IEE Proc. D Control Theory Appl.*, vol. 138, no. 3, p. 256, 1991, doi: [10.1049/ip-d.1991.0036](https://doi.org/10.1049/ip-d.1991.0036).
- [69] W. Yang, J. Li, W. Peng, and A. Deng, "A rub-impact recognition method based on improved convolutional neural network," *Comput., Mater. Continua*, vol. 62, no. 3, pp. 283–299, 2020, doi: [10.32604/cmc.2020.07511](https://doi.org/10.32604/cmc.2020.07511).
- [70] T. Xiao, Y. Xu, K. Yang, J. Zhang, Y. Peng, and Z. Zhang, "The application of two-level attention models in deep convolutional neural network for fine-grained image classification," in *Proc. IEEE Conf. Comput. Vis. Pattern Recognit. (CVPR)*, Boston, MA, USA, Dec. 2015, pp. 842–850, doi: [10.1109/CVPR.2015.7298685](https://doi.org/10.1109/CVPR.2015.7298685).
- [71] J. Zhu, L. Fang, and P. Ghamisi, "Deformable convolutional neural networks for hyperspectral image classification," *IEEE Geosci. Remote Sens. Lett.*, vol. 15, no. 8, pp. 1254–1258, Aug. 2018, doi: [10.1109/LGRS.2018.2830403](https://doi.org/10.1109/LGRS.2018.2830403).
- [72] M. A. Zoran, R. S. Savastru, and D. M. Savastru, "Multi-precursors assessment of earthquakes by geospatial and ground data," *Proc. 6th Int. Conf. Remote Sens. Geoinformation Environ. (RSCy)*, Aug. 2018, Art. no. 1077311, doi: [10.1117/12.2324958](https://doi.org/10.1117/12.2324958).



**JYH-WOEI LIN** received the B.Sc. degree from the Department of Physics, Chung Yuan Christian University, Taoyuan City, Taiwan, in 1989, the M.Sc. degree from the Institute of Geophysics, National Central University, Taoyuan City, in 1991, the Ph.D. degree from the Institut für Geophysik, Clausthal-Zellerfeld, Technische Universität Clausthal, Germany, in 2000, and the Ph.D. degree from the Department of Electrical Engineering, Southern Taiwan University of Science and Technology, Tainan, Taiwan, in 2019. Since 2016, he has been with the Department of Electrical Engineering, Southern Taiwan University of Science and Technology. He is currently a Professor with the Binjiang College, Nanjing University of Information Science and Technology, Wuxi, China. Until 2019, he has published over 70 SCI (SCIE) and EI articles. His research interests include artificial intelligence, space physics, geophysics, medical sciences, and remote sensing; especially four books publications in Germany and two books in USA.



**JUING-SHIAN CHIOU** received the B.S. degree from the Department of Electrical Engineering, Feng Chia University, Taiwan, and the M.S. degree from the Department of Electrical Engineering, National Central University, Taiwan, in 1986 and 1990, respectively, and the Ph.D. degree from the Department of Electrical Engineering, National Cheng Kung University, Tainan, Taiwan, in 2000. In 2000, he joined the Department of Electrical Engineering, Southern Taiwan University of Science and Technology, Tainan, where he is currently a Distinguished Professor and also the Vice-President of Taiwan Association for Academic Innovation. He has published over 60 articles. His research interests include artificial intelligence fuzzy control, unmanned aerial vehicles, algorithm, large-scale systems, hybrid systems, and geoscience.

...